How to cite: *Angew. Chem. Int. Ed.* **2021**, *60*, 9296–9300
International Edition: doi.org/10.1002/anie.202100456
German Edition: doi.org/10.1002/ange.202100456

Metal–Organic Frameworks **Hot Paper**

Amine-Tagged Fragmented Ligand Installation for Covalent Modification of MOF-74

Jaewoong Lim, Seonghwan Lee, Hyeonbin Ha, Junmo Seong, Seok Jeong, Min Kim, Seung Bin Baek, and Myoung Soo Lah**

Abstract: *MOF-74 is one of the most explored metal–organic frameworks (MOFs), but its functionalization is limited to the dative post-synthetic modification (PSM) of the monodentate solvent site. Owing to the nature of the organic ligand and framework structure of MOF-74, the covalent PSM of MOF-74 is very demanding. Herein, we report, for the first time, the covalent PSM of amine-tagged defective Ni-MOF-74, which is prepared by de novo solvothermal synthesis by using aminosalicylic acid as a functionalized fragmented organic ligand. The covalent PSM of the amino group generates metal binding sites, and subsequent post-synthetic metalation with Pd^{II} ions affords the Pd^{II}-incorporated Ni-MOF-74 catalyst. This catalyst exhibits highly efficient, size-selective, and recyclable catalytic activity for the Suzuki–Miyaura cross-coupling reaction. This strategy is also useful for the covalent modification of amine-tagged defective Ni_2(DOBPDC), an expanded analogue of MOF-74.*

MOF-74 is one of the most studied metal–organic frameworks (MOFs) because it is highly stable in various solvents and has a high density of potential open metal sites in the framework.[1–6] The dative post-synthetic modification (PSM) of the MOF-74 monodentate solvent site (i.e. the potential open metal site) has given it enhanced performance in various applications, such as gas storage,[7] selective separation,[8] and proton conductivity.[9] However, only a few applications in solution have been reported[10–12] because the ligand bound to the open metal site is released in the solution,[13] nullifying the dative PSM. The covalent PSM of MOF-74 is expected to give MOF-74 new physical and chemical properties that have not been reported so far, which will open up new opportunities in unexplored fields. However, the covalent PSM of MOF-74 is challenging because the synthesis of functionalized 2,5-dioxido-1,4-benzenedicarboxylic acid (H_4DOBDC) is very difficult. Moreover, the introduction of functionalized DOBDC is likely to increase steric hindrance between adjacent functionalized DOBDCs, inhibiting the formation of the isoreticular framework. Therefore, no covalent PSM of MOF-74 has been reported so far.

Herein, we report, for the first time, the covalent modification of amine-tagged defect-engineered Ni-MOF-74 (DEMOF-I) and Ni_2(DOBPDC)[14] (DEMOF-II, Scheme 1; $DOBPDC^{4-}$ = 4,4′-dioxido-3,3′-biphenyldicarboxylate). The introduction of amino groups into the MOF was achieved by direct solvothermal synthesis using *n*-aminosalicylic acid (H_2n-aSA) as a fragmented organic ligand. The amine-tagged DEMOF-I retains its crystallinity and permanent porosity even with defect sites in the framework. Below the approximated 20% doping level of *n*-aminosalicylate (n-aSA), all the MOFs showed an improved adsorption capacity for N_2. By covalent PSM, the amino group of DEMOF-I was converted into an iminopyridine group by reaction with pyridine aldehyde. Subsequent post-synthetic metalation produced a Pd^{II}-incorporated catalyst. The catalyst showed highly

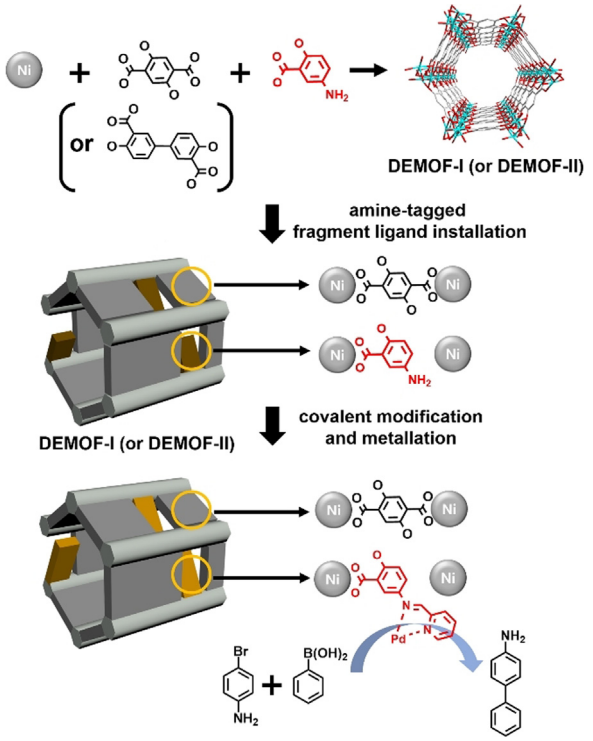

Scheme 1. Covalent modification and metalation of DEMOF-I (or DEMOF-II) prepared by a de novo solvothermal reaction by employing the mixed ligands DOBDC (or DODPDC) and an amine-tagged fragment, and the Suzuki–Miyaura cross-coupling reaction using Pd-incorporated DEMOF-I as a heterogeneous catalyst.

[*] J. Lim, S. Lee, J. Seong, Dr. S. Jeong, Prof. Dr. S. B. Baek, Prof. Dr. M. S. Lah
Department of Chemistry
Ulsan National Institute of Science and Technology (UNIST)
Ulsan 44919 (Republic of Korea)
E-mail: sbbaek@unist.ac.kr
mslah@unist.ac.kr
H. Ha, Prof. Dr. M. Kim
Department of Chemistry, Chungbuk National University
Cheongju 28644 (Republic of Korea)
Supporting information and the ORCID identification numbers for some of the authors of this article can be found under: https://doi.org/10.1002/anie.202100456.

efficient, size-selective, and recyclable catalytic performance for the Suzuki–Miyaura cross-coupling reaction of phenylboronic acid and a series of aryl bromides.

A fragmented ligand is often used either as a modulator[15,16] or as a defect-generating dopant[16–18] during the synthesis of MOFs. Since MOF-74 does not allow functionalized DOBDC in the framework, we used a functionalized DOBDC fragment as a dopant during the de novo synthesis of the amine-tagged defective MOF-74. Recently, several mixed-ligand M-MOF-74 (M = Mg, Mn, Co, and Ni) derivatives have been synthesized by doping 2-hydroxy-1,4-benzenedicarboxylate (BDC-OH).[19–21] Conversely, fragmented carboxylate ligands without hydroxy groups can only be doped into the framework at very low concentrations. This suggests that the two functional groups of DOBDC, namely -OH and -COOH, are required to participate simultaneously in the assembly of the mixed-ligand M-MOF-74. However, attempts to coassemble salicylate (SA) in Mn-MOF-74 was not successful.[20] Meanwhile, in the reaction of zinc and H_4DOBDC in the presence of salicylic acid (H_2SA), the H_2SA only acted as a modulator, and Zn-MOF-74 grew in the form of a nanosized rod.[22] With this information, we attempted to find doping conditions, using H_2SA as a fragmented ligand, since many salicylic acid derivatives with diverse functional groups are available. As functionalized fragments, we judiciously chose 5- and 3-aminosalicylic acid because an amino group is suitable for further covalent PSM with many organic functional groups.[23,24]

All attempts to incorporate an SA, as a fragmented ligand, into the framework of M-MOF-74 (M = Mg, Mn, Co, and Zn) were unsuccessful (Figures S1 and S2). In contrast, in the case of Ni-MOF-74, the SA-incorporated DEMOF-I (**I-SA$_x$**, where **I** and **x** represent Ni-MOF-74 and the mole fraction of the integrated SA at the DOBDC ligand sites of the framework, respectively) was successfully synthesized in a DMF/EtOH/H_2O (15:1:1, v/v/v) solvent mixture (Figures S3–S10). This approach is also effective for introducing 3-aSA or 5-aSA into the framework of Ni-MOF-74, thereby resulting in amine-tagged DEMOF-I (denoted as **I-n-aSA$_x$**, where **n-aSA** and **x** represent the integrated n-aSA and the mole fraction of the integrated n-aSA at the DOBDC sites of the framework, respectively). **I-SA$_x$** and **I-5-aSA$_x$** retained good crystallinity up to a fragment mole fraction of approximately 20% (Figures 1a, S5, and S11), whereas **I-3-aSA$_x$** retained its crystallinity, but its crystallinity was inferior to **I-SA$_x$** and **I-5-aSA$_x$** (Figures S6, S12, and S13).

As expected, the doping of the fragment affected the porosities of the resulting amine-tagged DEMOF-I. Interestingly, the doping of 5-aSA led to an increase in the porosity of **I-5-aSA$_x$** compared to pristine Ni-MOF-74 (Figure 1b and Table S1), even above a doping level of 30%. In contrast, the amount of N_2 absorbed in **I-SA$_x$** and **I-3-aSA$_x$** slightly increased only at relatively low mole fractions of fragments (Figures S14a, and S15a). The pristine Ni-MOF-74 and amine-tagged DEMOF-I showed almost the same mean pore diameters that peaked at 11 Å (Figures S14b, S15b, and S16). As the mole fraction of n-aSA increased, the pore-size distribution became wider, while the average pore dimension

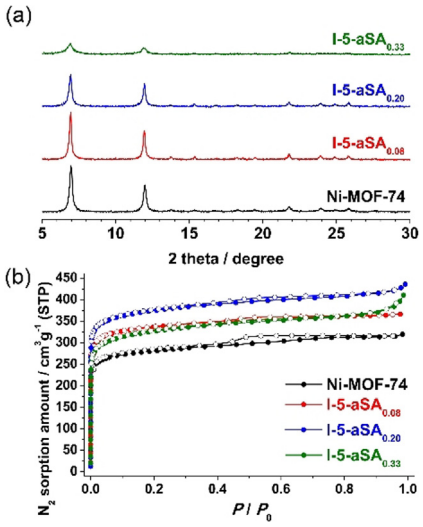

Figure 1. a) PXRD patterns and b) N_2 sorption isotherms of Ni-MOF-74 and **I-5-aSA$_x$** at 77 K.

was the same as that of the pristine Ni-MOF-74. This finding is related to the increase in the number of defect sites.

The amino group on **I-5-aSA$_{0.20}$** can be covalently modified through a Schiff-base condensation reaction. The reaction of **I-5-aSA$_{0.20}$** with 2-formylpyridine produced **I-5-pSA$_{0.20}$** containing a 5-(pyridin-2-ylmethylene)amino group (Figure S17a). The Pd-incorporated DEMOF-I, **I-5-pSA$_{0.20}$-Pd$_{0.05}$**, can be obtained through post-synthetic metalation.[25] The Pd-incorporated MOFs preserved their crystallinity after the entire PSM procedure (Figure 2a). Transmission electron microscopy (TEM) and energy-dispersive spectroscopy (EDS) showed that the Pd atoms were considerably dispersed in **I-5-pSA$_{0.20}$-Pd$_{0.05}$** (Figure 2c–e). **I-3-pSA$_{0.18}$** and **I-3-pSA$_{0.18}$-Pd$_{0.07}$** can also be obtained by the same procedure using **I-3-aSA$_{0.18}$** (Figures S17b, S18, and S19). X-ray photoelectron spectroscopy (XPS) data support the presence of Pd^{II} ions in **I-3-pSA$_{0.18}$-Pd$_{0.07}$** (Figure S20). The covalent PSM of the amine-tagged DEMOF-I and subsequent metalation of the framework slightly reduced the pore volume of the corresponding MOF (Figures 2b, S21a, and Table S1). The doping of n-aSA led to a significant broadening of the pore-size distribution of the MOFs (Figures S21b and S22), which suggests that the enlargement and reduction of the local pore dimension occurred simultaneously around the defect sites. More interestingly, the covalent PSM had a different effect on the pore-size distributions of the modified DEMOFs. The functionalization of both amine-substituted SAs led to a narrow pore-size distribution of the MOFs. Conversely, while the functionalization of the 3-aSA residue mainly reduced the size of the relatively large pores, the functionalization of the 5-aSA residue predominantly reduced the size of the relatively small pores. Thus, MOFs with different average pore dimensions were produced. The average pore size of **I-3-pSA$_{0.18}$-Pd$_{0.07}$** ($\approx$10 Å) and **I-5-pSA$_{0.20}$-Pd$_{0.05}$** ($\approx$12 Å) is slightly smaller and larger than that of the pristine Ni-MOF-74 ($\approx$11 Å), respectively.

Although there are no reports of the covalent modification of DOBPDC in Ni_2(DOBPDC), an extended analogue of

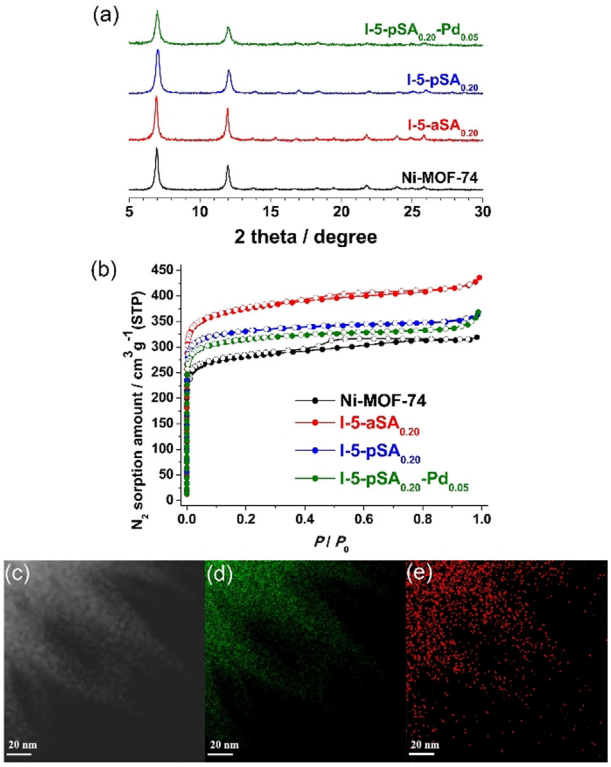

Figure 2. a) PXRD and b) N_2 sorption isotherms of **I-5-aSA$_{0.20}$**, **I-5-pSA$_{0.20}$**, and **I-5-pSA$_{0.20}$-Pd$_{0.05}$**. c) TEM image of **I-5-pSA$_{0.20}$-Pd$_{0.05}$**. EDS mappings of d) Ni (green) and e) Pd (red) overlaid on the TEM image of **I-5-pSA$_{0.20}$-Pd$_{0.05}$**.

MOF-74, which has larger pores than MOF-74, can provide a more efficient diffusion of a substrate or diffuse a larger substrate into its framework than MOF-74.[14,26–28] The same synthetic procedure was applied for the synthesis of DEMOF-II to determine whether the synthetic strategy was valid for the MOF-74 analogue. Following the same procedure used for the preparations of **I-SA$_x$** and **I-n-aSA$_x$** (Figures S23 and S24), amine-tagged DEMOF-II, denoted as **II-SA$_{0.10}$**, **II-5-aSA$_{0.05}$**, and **II-5-aSA$_{0.17}$**, depending on the incorporated fragments, was successfully synthesized using H_4DOBPDC. Additionally, the covalently modified DEMOF-II, **II-5-pSA$_{0.17}$** and **II-5-pSA$_{0.17}$-Pd$_{0.06}$**, were prepared according to the same covalent PSM procedure used for the preparation of **I-5-pSA$_{20}$** and **I-5-pSA$_{0.20}$-Pd$_{0.05}$**. The pore volume of **II-5-aSA$_{0.17}$** was significantly reduced compared to that of pristine Ni_2(DOBPDC) (Figure S25a and Table S1). The reduced porosity of the amine-tagged DEMOF-II might be related to the reduced crystallinity arising from the increased number of defect sites in the crystals. The presence of n-aSA in the framework altered the average pore size and pore-size distribution of the MOFs. The amine-tagged DEMOF-II had an average pore size of 17 Å, which is approximately 4 Å smaller than that of the pristine Ni_2(DOBPDC) (Figure S25b). The pore-size distribution of the amine-tagged DEMOF-II became wider and shifted towards a relatively small dimension. This indicates that the doping of n-aSA reduces pore dimensions around defect sites. Subsequent functionalization and Pd metalation slightly reduced the pore volume and pore dimensions of the functionalized and Pd-incorporated DEMOF-II, **II-5-pSA$_{0.17}$** and **II-5-pSA$_{0.17}$-Pd$_{0.06}$**.

Since the Pd^{II}-incorporated DEMOFs have a catalytic center in the framework, we performed the Suzuki–Miyaura cross-coupling reaction, one of the representative Pd-catalyzed reactions between aryl halides and aryl boronic acids,[29–31] to evaluate the catalytic activities of the Pd^{II}-incorporated DEMOFs. As a model reaction, 4-bromoaniline (substrate **1**) and phenylboronic acid were selected as the substrates to form 4-aminobiphenyl (Table 1). Whereas the pristine Ni-MOF-74, **I-5-aSA$_{0.20}$** and **I-5-pSA$_{0.20}$**, showed no catalytic activity (entry 1), **I-5-pSA$_{0.20}$-Pd$_{0.05}$** afforded a 99% yield of the cross-coupled product, 4-aminobiphenyl (entry 2). Interestingly, **I-5-pSA$_{0.20}$-Pd$_{0.05}$** exhibited superior catalytic activity compared to $PdCl_2$, a commercially available homogeneous catalyst, under the same reaction conditions. Additionally, the catalytic activity of **I-5-pSA$_{0.20}$-Pd$_{0.05}$** was equivalent to that of **Pd-5-pSA** (entry 5), a homogeneous model catalyst, whose structure imitates the catalytic site of **I-5-pSA$_{0.20}$-Pd$_{0.05}$**. The catalytic activities of **I-5-pSA$_{0.20}$-Pd$_{0.05}$** and **I-3-pSA$_{0.18}$-Pd$_{0.07}$** were also examined for the C–C coupling reaction of phenylboronic acid with various aryl bromides (Table S2). Both catalysts were highly efficient for the reactions. The yields ranged from 72% to 99%, depending on the substrate.

Table 1: Pd-catalyzed Suzuki–Miyaura cross-coupling reactions.

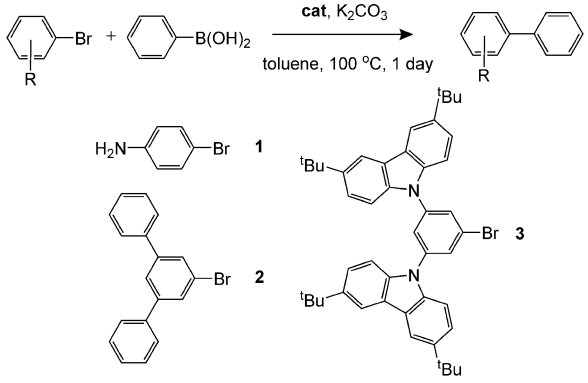

Entry	Catalyst[a]	Substrate	Yield[b] [%]
1	**I-5-pSA$_{0.20}$**	**1**	0
2	**I-5-pSA$_{0.20}$-Pd$_{0.05}$**		99
3	**I-3-pSA$_{0.18}$-Pd$_{0.07}$**[a]		99
4	**II-5-pSA$_{0.17}$-Pd$_{0.06}$**[a]		71
5	**Pd-5-pSA**		99
6	$PdCl_2$		60
7	**I-5-pSA$_{0.20}$-Pd$_{0.05}$**	**2**	80
8		**3**	30
9	**I-3-pSA$_{0.18}$-Pd$_{0.07}$**[a]	**2**	88
10		**3**	19
11	**II-5-pSA$_{0.17}$-Pd$_{0.06}$**[a]	**2**	80
12		**3**	53
13	**Pd-5-pSA**	**2**	99
14		**3**	99

[a] 1.3 mol% Pd for **I-5-pSA$_{0.20}$-Pd$_{0.05}$**; 2.0 mol% Pd for **I-3-pSA$_{0.18}$-Pd$_{0.07}$**; 2.3 mol% Pd for **II-5-pSA$_{0.17}$-Pd$_{0.06}$**; 1.3 mol% Pd for the other Pd-containing catalysts. [b] Yields were determined by ^{1}H NMR spectroscopy.

It is well-known that heterogeneous catalysts derived from MOFs can utilize the catalytic sites located at their outer and inner pore surfaces.[32,33] To elucidate the locations of active catalytic sites in the DEMOF-74 catalysts, we performed Suzuki–Miyaura coupling reactions of phenylboronic acid with aryl bromides of various molecular dimensions. The C–C coupling reactions of the smallest substrate 4-bromoaniline were quantitative (entries 2 and 3), except for with **II-5-pSA$_{0.17}$-Pd$_{0.06}$** (entry 4), which had the largest pore dimensions. The relatively low yield can be attributed to the low density of active catalytic centers in **II-5-pSA$_{0.17}$-Pd$_{0.06}$** compared to the other catalysts investigated. For 1-bromo-3,5-diphenylbenzene (substrate **2**), where the second-largest minimum dimension (MIN-2, 10.8 Å) is similar to the pore dimension of **I-3-pSA$_{0.18}$-Pd$_{0.07}$**, the yields ranged from 80 % to 88 % for the same heterogeneous catalysts (entries 7, 9, and 11). These yields contrast with the completion of the reaction with the homogeneous catalyst **Pd-5-pSA** (entry 13).

The size-selectivity of the catalysts is demonstrated in the reaction of 9,9′-(5-bromo-1,3-phenylene)bis(3,6-di-*tert*-butyl-9*H*-carbazole (substrate **3**). The molecular dimensions of substrate **3** (MIN-2, 13.5 Å) is comparable to the pore dimensions of **I-5-pSA$_{0.20}$-Pd$_{0.05}$** and slightly larger than that of **I-3-pSA$_{0.18}$-Pd$_{0.07}$**. Additionally, the MIN-2 of the C–C coupled product was estimated to be 17.4 Å, which is considerably larger than the pore dimensions of both catalysts. As expected, we observed drastically reduced catalytic activities with a 30 % yield for **I-5-pSA$_{0.20}$-Pd$_{0.05}$** (entry 8) and 19 % yield for **I-3-pSA$_{0.18}$-Pd$_{0.07}$** (entry 10). The C–C coupling reactions were expected to occur mainly at the catalytic sites located on the outer surface of the MOFs. Meanwhile, the yield of the same reaction with **II-5-pSA$_{0.17}$-Pd$_{0.06}$**, at 53 %, was significantly enhanced (entry 12) because the catalytic sites at the outer surface and inner pore surface of **II-5-pSA$_{0.17}$-Pd$_{0.06}$** with an average pore size of 17 Å were more accessible to the substrate.

The leaching of metal ions from the active sites during catalysis is a critical issue for metal-incorporated heterogeneous catalysts.[29,34] Therefore, a hot-filtration test was performed using the reaction of **I-5-pSA$_{0.20}$-Pd$_{0.05}$** to determine whether Pd ions were leached out during the reaction. After 1 h of reaction, the catalyst **I-5-pSA$_{0.20}$-Pd$_{0.05}$** was removed from the reaction mixture by hot filtration, and the filtrate was allowed to react for an additional 23 h. The undisturbed C–C coupling reaction was almost complete after 24 h. In contrast, once the catalyst was removed by filtration, the reaction stopped, indicating the absence of Pd ions in the filtrate (Figure 3a). Inductively coupled plasma optical emission spectrometry (ICP-OES) for Pd content also supported the absence of Pd in the filtrate, where the detected Pd content was below the detection limit of the instrument. The stability and recyclability of heterogeneous catalysts are very important for practical applications. To evaluate the recyclability of the catalyst, **I-5-pSA$_{0.20}$-Pd$_{0.05}$** was recovered from the reaction mixture by centrifugation, and the recovered catalyst was used in successive runs of the Suzuki–Miyaura cross-coupling reaction. No decrease in catalytic activity (> 99 % yield) was observed, even after the fifth reaction, thus indicating the relatively high stability of the catalyst under the reaction conditions (Figure 3b). The PXRD characterization of **I-5-pSA$_{0.20}$-Pd$_{0.05}$** after catalysis further demonstrated that the Pd^{II}-incorporated DEMOF, **I-5-pSA$_{0.20}$-Pd$_{0.05}$**, retained high crystallinity (Figure S26).

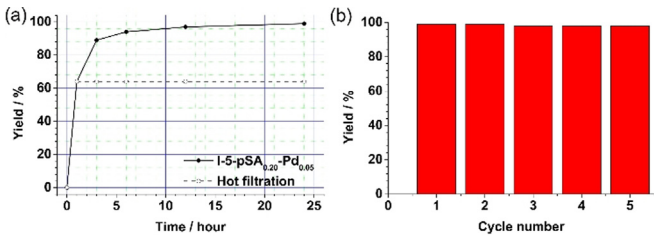

Figure 3. a) Hot filtration and b) recycling test of **I-5-pSA$_{0.20}$-Pd$_{0.05}$** in the Suzuki–Miyaura cross-coupling reaction.

In summary, we have successfully demonstrated that the synthesis of functionalized DEMOF-I and DEMOF-II derivatives can be achieved by amine-tagged fragment installation. The installation of the fragment into the framework resulted in defective but highly stable porous MOFs. Amine-tagged DEMOFs can be covalently modified with an aldehyde functional group to give an iminopyridine functionality that can be further modified by post-synthetic metalation. The Pd-incorporated DEMOFs were highly efficient, size-selective, and recyclable heterogeneous catalysts for the Suzuki–Miyaura cross-coupling reaction. These results suggest that a combination of fragment installation and subsequent covalent PSM will become an efficient procedure to introduce desired functionality into MOFs, and this approach will provide great opportunities to explore many MOFs in diverse applications.

Acknowledgements

This work was supported by grants (2016R1A5A1009405 and 2019R1I1A1A01062148) from the National Research Foundation (NRF) of Korea.

Conflict of interest

The authors declare no conflict of interest.

Keywords: covalent modification · fragmented ligands · heterogeneous catalysis · metal-organic frameworks · post-synthetic modification

[1] N. L. Rosi, J. Kim, M. Eddaoudi, B. Chen, M. O'Keeffe, O. M. Yaghi, *J. Am. Chem. Soc.* **2005**, *127*, 1504 – 1518.
[2] S. R. Caskey, A. G. Wong-Foy, A. J. Matzger, *J. Am. Chem. Soc.* **2008**, *130*, 10870 – 10871.
[3] E. D. Bloch, L. J. Murray, W. L. Queen, S. Chavan, S. N. Maximoff, J. P. Bigi, R. Krishna, V. K. Peterson, F. Grandjean, G. J. Long, B. Smit, S. Bordiga, C. M. Brown, J. R. Long, *J. Am. Chem. Soc.* **2011**, *133*, 14814 – 14822.
[4] Y. He, R. Krishna, B. Chen, *Energy Environ. Sci.* **2012**, *5*, 9107 – 9120.

[5] Ü. Kökçam-Demir, A. Goldman, L. Esrafili, M. Gharib, A. Morsali, O. Weingart, C. Janiak, *Chem. Soc. Rev.* **2020**, *49*, 2751 – 2798.
[6] T. Xiao, D. Liu, *Microporous Mesoporous Mater.* **2019**, *283*, 88 – 103.
[7] A. C. McKinlay, B. Xiao, D. S. Wragg, P. S. Wheatley, I. L. Megson, R. E. Morris, *J. Am. Chem. Soc.* **2008**, *130*, 10440 – 10444.
[8] J. Y. Kim, R. Balderas-Xicohténcatl, L. Zhang, S. G. Kang, M. Hirscher, H. Oh, H. R. Moon, *J. Am. Chem. Soc.* **2017**, *139*, 15135 – 15141.
[9] M. K. Sarango-Ramírez, D.-W. Lim, D. I. Kolokolov, A. E. Khudozhitkov, A. G. Stepanov, H. Kitagawa, *J. Am. Chem. Soc.* **2020**, *142*, 6861 – 6865.
[10] D.-A. Yang, H.-Y. Cho, J. Kin, S.-T. Yang, W.-S. Ahn, *Energy Environ. Sci.* **2012**, *5*, 6465 – 6473.
[11] D. Wu, Z. Guo, X. Yin, Q. Pang, B. Tu, L. Zhang, Y.-G. Wang, Q. Li, *Adv. Mater.* **2014**, *26*, 3258 – 3262.
[12] P. Valvekens, M. Vandichel, M. Waroquier, V. V. Speybroeck, D. D. Vos, *J. Catal.* **2014**, *317*, 1 – 10.
[13] H. Kim, M. Sohail, K. Yim, Y. C. Park, D. H. Chun, H. J. Kim, S. O. Han, J.-H. Moon, *ACS Appl. Mater. Interfaces* **2019**, *11*, 7014 – 7021.
[14] T. M. McDonald, W. R. Lee, J. A. Mason, B. M. Wiers, C. S. Hong, J. R. Long, *J. Am. Chem. Soc.* **2012**, *134*, 7056 – 7065.
[15] J. Park, Q. Jiang, D. Feng, L. Mao, H.-C. Zhou, *J. Am. Chem. Soc.* **2016**, *138*, 3518 – 3525.
[16] G. C. Shearer, S. Chavan, S. Bordiga, S. Svelle, U. Olsbye, K. P. Lillerud, *Chem. Mater.* **2016**, *28*, 3749 – 3761.
[17] J. Park, Z. U. Wang, L.-B. Sun, Y.-P. Chen, H.-C. Zhou, *J. Am. Chem. Soc.* **2012**, *134*, 20110 – 20116.
[18] Z. Fang, J. P. Dürholt, M. Kauer, W. Zhang, C. Lochenie, B. Jee, B. Albada, N. Metzler-Nolte, A. Pöppl, B. Weber, M. Muhler, Y. Wang, R. Schmid, R. A. Fischer, *J. Am. Chem. Soc.* **2014**, *136*, 9627 – 9636.
[19] N. E. A. El-Gamel, *Eur. J. Inorg. Chem.* **2015**, 1351 – 1358.
[20] D. Wu, W. Yan, H. Xu, E. Zhang, Q. Li, *Inorg. Chim. Acta* **2017**, *460*, 93 – 98.
[21] J. A. Villajos, N. Jagorel, S. Reinsch, F. Emmerling, *Front. Mater.* **2019**, *6*, 230.
[22] P. Pachfule, D. Shinde, M. Majumder, Q. Xu, *Nat. Chem.* **2016**, *8*, 718 – 724.
[23] Z. Wang, S. M. Cohen, *Angew. Chem. Int. Ed.* **2008**, *47*, 4699 – 4702; *Angew. Chem.* **2008**, *120*, 4777 – 4780.
[24] Z. Yin, S. Wan, J. Yang, M. Kurmoo, M.-H. Zeng, *Coord. Chem. Rev.* **2019**, *378*, 500 – 512.
[25] C. J. Doonan, W. Morris, H. Furukawa, O. M. Yaghi, *J. Am. Chem. Soc.* **2009**, *131*, 9492 – 9493.
[26] T. M. McDonald, J. A. Mason, X. Kong, E. D. Bloch, D. Gygi, A. Dani, V. Crocellà, F. Giordanino, S. O. Odoh, W. S. Drisdell, B. Vlaisavljevich, A. L. Dzubak, R. Poloni, S. K. Schnell, N. Planas, K. Lee, T. Pascal, L. F. Wan, D. Prendergast, J. B. Neaton, B. Smit, J. B. Kortright, L. Gagliardi, S. Bordiga, J. A. Reimer, J. R. Long, *Nature* **2015**, *519*, 303 – 308.
[27] M. L. Aubrey, R. Ameloot, B. M. Wiers, J. R. Long, *Energy Environ. Sci.* **2014**, *7*, 667 – 671.
[28] H. M. Tay, A. Rawal, C. Hua, *Chem. Commun.* **2020**, *56*, 14829 – 14832.
[29] X. Li, R. V. Zeeland, R. V. Maligal-Ganesh, Y. Pei, G. Power, L. Stanley, W. Huang, *ACS Catal.* **2016**, *6*, 6324 – 6328.
[30] H. Fei, S. M. Cohen, *Chem. Commun.* **2014**, *50*, 4810 – 4812.
[31] G. Xiong, X.-L. Chen, L.-X. You, B.-Y. Ren, F. Ding, I. Dragutan, V. Dragutan, Y.-G. Sun, *J. Catal.* **2018**, *361*, 116 – 125.
[32] S. Kim, J. Lee, S. Jeoung, H. R. Moon, M. Kim, *Chem. Eur. J.* **2020**, *26*, 7568 – 7572.
[33] D. Yang, B. C. Gates, *ACS Catal.* **2019**, *9*, 1779 – 1798.
[34] I. Hussain, J. Capricho, M. A. Yawer, *Adv. Synth. Catal.* **2016**, *358*, 3320 – 3349.

Manuscript received: January 11, 2021
Version of record online: March 5, 2021

